Charge Inhomogeneity Determines Oxidative Reactivity of Graphene on Substrates

Mahito Yamamoto, Theodore L. Einstein, Michael S. Fuhrer,* and William G. Cullen

Materials Research Science and Engineering Center and Center for Nanophysics and Advanced Materials, Department of Physics, University of Maryland, College Park, Maryland 20742-4111, United States

ABSTRACT

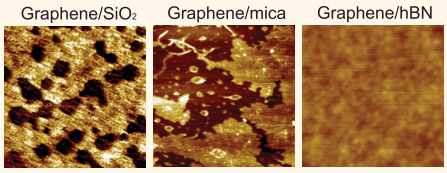

After oxygen treatment at 500 °C

Single-layer graphene (SLG) supported on SiO_2 shows anomalously large chemical reactivity compared to thicker graphene, with charge inhomogeneity-induced potential fluctuations or topographic corrugations proposed as the cause. Here we systematically probe the oxidative reactivity of graphene supported on substrates with different surface roughnesses and charged impurity densities: hexagonal boron nitride (hBN), mica, thermally grown SiO_2 on Si, and SiO_2 nanoparticle thin films. SLG on low charge trap density hBN is not etched and shows little doping after oxygen treatment at temperatures up to 550 °C, in sharp contrast with oxidative etching under similar conditions of graphene on high charge trap density SiO_2 and mica. Furthermore, bilayer graphene shows reduced reactivity compared to SLG regardless of its substrate-induced roughness. Together the observations indicate that graphene's reactivity is predominantly controlled by charge inhomogeneity-induced potential fluctuations rather than surface roughness.

KEYWORDS: graphene · reactivity · oxidation · hexagonal boron nitride · mica · Raman spectroscopy

Chemical functionalization and doping of graphene have been of great interest as an approach to tailoring its electronic structure.[1−3] Covalent functionalization changes the hybridization of carbon bonds from sp^2 to sp^3, leading to significant alteration of electronic properties of graphene. For example, graphene can be covalently functionalized with atomic hydrogen[4,5] and the hydrogenation of graphene results in "graphane" which exhibits insulating behavior in contrast to semimetallic graphene.[5] Additionally, fluorination has been observed to lead to a wide band gap[6,7] and paramagnetism[8] in graphene. Chemical doping offers a route to larger carrier concentrations in graphene than can be achieved by electrical gating.[9] Understanding graphene's chemical reactivity is a crucial step toward chemically engineering graphene's electronic properties.

Pristine graphene is relatively inert chemically because of the absence of dangling bonds; in contrast, graphene nanoribbons[10] and graphene with defects[11] are reactive. Nonetheless, single-layer graphene (SLG) supported on SiO_2 shows anomalously large reactivity compared to thicker graphene.[12−14] One possible explanation for this enhanced reactivity is Fermi energy fluctuations in space, that is, "electron-hole puddles",[15,16] induced in graphene due to ionized impurities trapped on SiO_2, which limit the carrier mobility of graphene.[17−19] The electron−hole puddles locally increase the electron (hole) density responsible for electron transfer chemistry.[13] The magnitude of the potential fluctuations and, hence, the the charged impurity-assisted electron transfer decrease with increasing graphene thickness because of (1) higher density of states in multilayer graphene[20] and (2) interlayer screening of charged impurities, where the screening length corresponds to the thickness of bilayer to few-layer graphene.[13,21,22]

Another plausible mechanism for the enhancement of the reactivity is topographic corrugations of graphene induced by coupling to the SiO_2 surface.[13,23] Due to van der Waals adhesion, graphene deforms significantly on SiO_2,[24,25] resulting in local curvature and strain. The curvature may lead to the rehybridization of sp^2 to sp^3 bonds[26] and enhanced reactivity. The impact of the structural deformations on the reactivity is also expected to attenuate with increasing graphene thickness because graphene layers become significantly stiffer and flatter over SiO_2,[27,28] with curvature and strain

* Address correspondence to mfuhrer@umd.edu.

Received for review July 10, 2012 and accepted August 23, 2012.

Published online August 23, 2012
10.1021/nn303082a

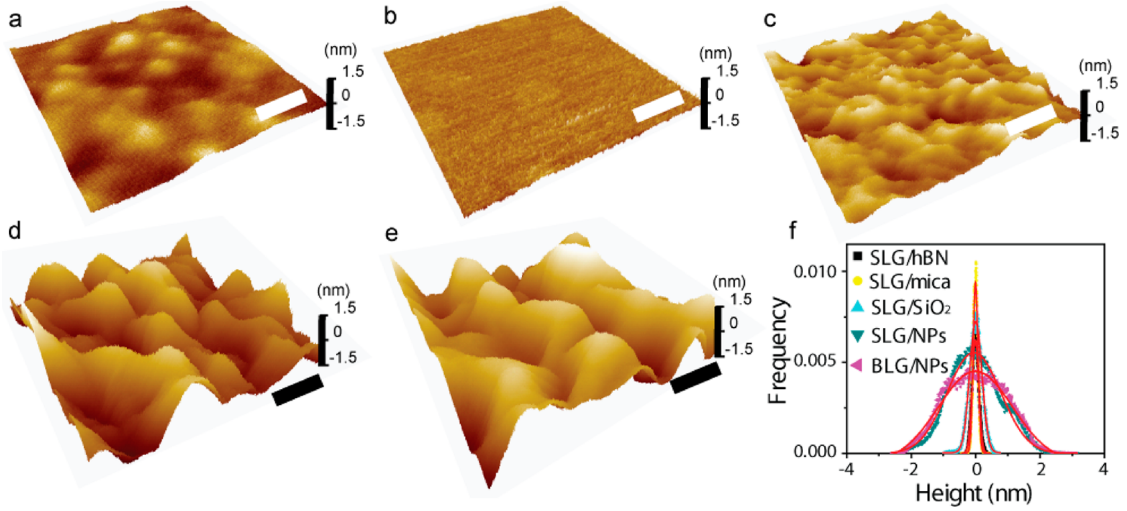

Figure 1. Typical AFM images of SLG supported on (a) hBN, (b) mica, (c) SiO_2, (d) a SiO_2 nanoparticle thin film, and (e) BLG on a SiO_2 nanoparticle thin film. Scale bars are 40 nm. (f) Height histograms of graphene surfaces for the images shown in panels a–e. Solid red lines are Gaussian fits.

decreasing with thickness. Since SiO_2 induces both significant charge fluctuations[15,16] and structural deformations[24,25] in SLG, either could account for the enhancement of reactivity of SLG on SiO_2.[13,29]

Here, we report a systematic study of the oxidative reactivity of graphene supported on various substrates with different surface roughnesses and charged impurity densities: hexagonal boron nitride (hBN), mica, thermally grown SiO_2 on Si, and SiO_2 nanoparticle thin films. hBN has gained increasing interest as a "clean" substrate for graphene electronic devices. Graphene supported on hBN is atomically flat,[30,31] has remarkably high carrier mobility,[32] and shows significantly reduced charge inhomogeneity, presumably due to lower concentrations of substrate-trapped charge.[30,31] Muscovite mica is expected to possess significant concentrations of K^+ ions on its surface,[33] and SLG on mica exhibits comparable carrier mobility to that of SiO_2-supported SLG,[34] implying similar concentrations of substrate-trapped charge. Furthermore, the cleavage of mica exposes a silicate face,[33] chemically very similar to amorphous SiO_2. Thus, in common with SiO_2, graphene is supposedly nonreactive to the mica surface. However, graphene deposited on mica is exceedingly flat.[35] SiO_2 nanoparticles on a SiO_2 substrate produce a graphene support with significantly higher roughness than, but similar chemical properties to, thermally grown SiO_2 on Si.

We find that SLG on hBN is remarkably inert in reaction with oxygen, unlike SiO_2-supported graphene and atomically flat graphene on mica. Graphene on mica is significantly hole-doped and etched by oxidation, and the reactivity decreases with graphene thickness. These results indicate that differences in substrate charged-impurity concentrations, not roughness, account for the differences in reactivity. Additionally, we find that bilayer graphene (BLG) on a SiO_2 nanoparticle thin film shows greater surface roughness yet significantly lower chemical reactivity than SLG on SiO_2, providing additional corroboration that roughness is not a major factor determining chemical reactivity.

RESULTS AND DISCUSSION

hBN flakes were exfoliated onto Si substrates with a 300 nm oxide layer from commercially available BN powder (Momentive, Polartherm grade PT 110).[36] Muscovite mica was cleaved in a N_2 atmosphere to minimize the chance of a water layer on the mica surface.[35,37] SiO_2 nanoparticle thin films were prepared by spin-coating SiO_2 nanoparticle dispersions (diameter 10–20 nm; Nissan Chemical America Corp., SNOWTEX-O) onto SiO_2 substrates. Graphene was mechanically exfoliated onto these substrates from Kish graphite (see Methods for details). The samples were then annealed in an Ar/O_2 mixture for 2–5 h at temperatures ranging from 350 to 600 °C. We employed atomic force microscopy (AFM) in ambient and Raman spectroscopy with a fixed laser wavelength of 532 nm unless otherwise noted to characterize the oxidative reactivity of graphene on substrates.

Figure 1 images a–d show typical AFM topographic images of SLG supported on (a) hBN (thickness of ~9 nm supported on SiO_2), (b) mica, (c) SiO_2, (d) SiO_2 nanoparticles. Additionally, Figure 1e shows an AFM image of BLG on SiO_2 nanoparticles. These samples were annealed in Ar/H_2 flow at 400 °C for 6 h to remove any adhesive residue and achieve equilibrium structures but not exposed to oxidative treatment. Figure 1f shows the height histograms of the images in Figure 1a–e; mica-supported graphene is the flattest, followed by graphene on hBN, SiO_2, and SiO_2 nanoparticles. Table 1 summarizes the root-mean-square (rms) roughness σ and the characteristic length l of

TABLE 1. The RMS Roughness σ, Characteristic Length l, Estimated Curvature σ/l^2, and Strain $(\sigma/l)^2$ of SLG on hBN, Mica, SiO_2, and SiO_2 Nanoparticles (NPs) and BLG on NPs

	SLG/hBN	SLG/mica	SLG/SiO_2	SLG/NPs	BLG/NPs
σ (nm)	0.14 ± 0.04	0.05 ± 0.02	0.23 ± 0.01	1.29 ± 0.12	1.30 ± 0.11
l (nm)	24 ± 11	1.7 ± 0.6	13 ± 2	21 ± 5	22 ± 4
σ/l^2 ($\times 10^{-4}$ nm^{-1})	2.4 ± 2.2	N/A	14 ± 5	30 ± 15	27 ± 10
$(\sigma/l)^2$ ($\times 10^{-5}$)	3.2 ± 3.5	N/A	31 ± 11	389 ± 208	352 ± 145

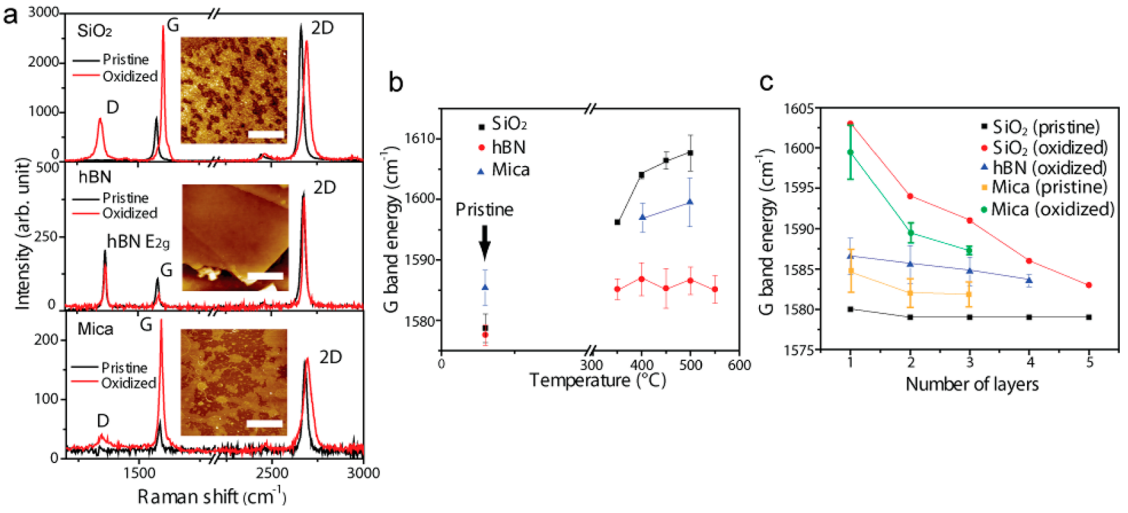

Figure 2. (a) Raman spectra of SLG on SiO_2 (top), hBN (middle), and mica (bottom) before and after oxidation at 500 °C for 2 h. Raman spectra are normalized to the 2D peak intensities. Insets are typical AFM of SLG on the substrates after oxidation at 500 °C for 2 h. Scale bars are 1 μm. (b) Raman G band energies of SLG on SiO_2 (black square dots), hBN (red circular dots), and mica (blue triangular dots) as functions of oxygen treatment temperature. (c) Raman G band energies of pristine graphene on SiO_2 (black square dots) and on mica (yellow square dots) and 500 °C-oxidized graphene on SiO_2 (red circular dots), on hBN (blue triangular dots), and on mica (green circular dots) as functions of number of graphene layers.

graphene surfaces (see Supporting Information for the formal definitions of σ and l). Since graphene on mica is exceedingly flat, we expect that the rms roughness and the characteristic length reflect the AFM height resolution limit and AFM noise, respectively, as previously noted.[35] To quantitatively assess the deformations present in graphene, we roughly estimate curvature and strain by σ/l^2 and $(\sigma/l)^2$ as shown in Table 1. By relative comparison, we find much larger deformations in SLG and BLG on SiO_2 nanoparticles than SLG on SiO_2. We cannot exclude, however, that nanometer-scale substrate roughness produces sharp mechanical deformations (conical singularities) in graphene, which would be unresolved by our tapping-mode AFM. These localized deformations are expected to significantly perturb the local density of states of graphene near the apex[38] and consequently may contribute to reactivity of graphene.

Figure 2a shows typical Raman spectra of graphene supported on SiO_2, hBN, and mica before (black solid line) and after (red solid line) oxidation at 500 °C for 2 h. Previous studies of graphene oxidation have reported hole-doping and disorder in reactions with oxygen.[12,39,40] On SiO_2, we find that the Raman G band upshifts from ~1582 to 1603 cm^{-1}, which roughly corresponds to a dopant concentration of $\sim 2 \times 10^{13}$ cm^{-2}.[12,41,42] Additionally, the Raman D peak at ~1350 cm^{-1} is activated after oxidation because of formation of etch pits (see inset), as previously reported.[12] On hBN the upshift of the G band energy is minor (from 1580 cm^{-1} to 1585 cm^{-1}); furthermore, the Raman D peak is absent, indicating that doping in graphene is significantly suppressed and graphene is not etched, as can be seen in the middle inset (hBN shows the E_{2g} Raman mode[43] at ~1360 cm^{-1} but this nondispersive mode can be distinguished from the dispersive graphene D mode by using longer-wavelength excitation; see below and Supporting Information). The suppression of the reactivity of graphene was consistently observed on hBN for all samples at oxidative temperatures below 550 °C (we obtained no samples of hBN thickness less than 9 nm). Etching of graphene on hBN requires a higher oxidative temperature. At 600 °C, oxidative etching proceeds very rapidly at the edges or pits, and graphene is almost completely etched after 2 h oxidation. In contrast to hBN-supported SLG, SLG on mica is partly etched by oxidation as shown in the bottom inset (see also Supporting Information for height profiles of the AFM images), which is also evidenced by the Raman D peak.

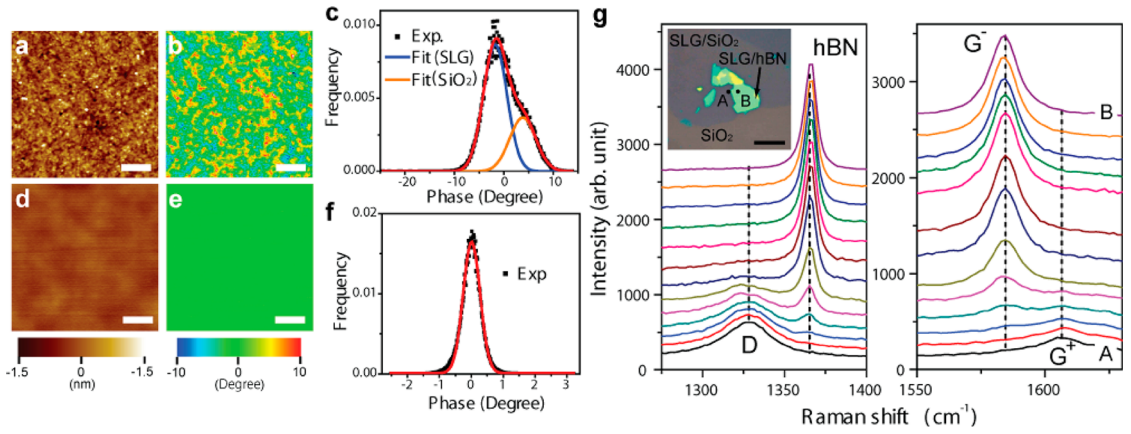

Figure 3. AFM (a) height and (b) phase images of SLG on SiO_2 shown in the inset of panel g after oxidation at 450 °C for 5 h. Scale bars are 200 nm. (c) Histogram of phase variations in panel b. The red solid line is a multipeak Gaussian fit, consisting of two peaks derived from graphene (blue) and SiO_2 (orange) surfaces. AFM (d) height and (e) phase images of SLG on hBN after oxidation at 450 °C for 5 h. Scale bars are 200 nm. (f) Phase histogram image e. Solid line is a Gaussian fit. (g) Series of Raman spectra of SLG taken from point A (on SiO_2) to point B (on hBN) as shown in inset. The spacing between points at which the Raman spectra are measured is 0.3 μm. Inset is an optical image of SLG supported on SiO_2 and hBN. Scale bar is 10 μm.

In Figure 2b, we plot the Raman G band energies of SiO_2-, hBN-, and mica- supported SLG as functions of temperature. The relatively large G band energy of pristine SLG on mica results from hole doping by preexisting surface charges on the substrate.[44] The G band energies of SLG on SiO_2 and on mica increase with increasing temperature, indicating doping due to reactivity to oxygen molecules, while hBN-supported graphene shows a nearly constant G band energy of $\sim$1585 cm^{-1} at 350−550 °C, indicating little doping. We also examine the G band energy as a function of graphene thickness in Figure 2c. On SiO_2 and on mica, SLG shows the largest G-band shift (largest doping) and the G-band energies diminish with thickness, indicating larger reactivity of SLG compared to thicker graphenes, while the G-band shift for graphene on hBN does not depend on thickness. These observations suggest SLG on hBN is comparable to thick graphene in terms of oxidative doping.

In Figure 3 we further investigate the reactivity of graphene on hBN in terms of oxidative etching. As oxidation progresses, graphene on SiO_2 is significantly etched as evidenced by the appearance of a D-band in the Raman spectrum (see Figure 3g). After oxidation at 450 °C for 5 h, graphene strongly couples to SiO_2, making it difficult to distinguish graphene and uncovered SiO_2 from an AFM height image (Figure 3a). We therefore use AFM phase imaging (Figure 3b) to distinguish SLG from etched regions. The phase image clearly shows variations, indicating that the scanned region is compositionally inhomogeneous. In Figure 3c, we show the phase histogram of the image shown in Figure 3b. The multipeak Gaussian fit of the histogram consists of two components: the smaller peak corresponds to graphene, while the larger peak corresponds to uncovered SiO_2 where SLG has been etched (see Supporting Information for a phase image at edges of pristine graphene on SiO_2). Figure 3 panels d and e show AFM height and phase images of SLG on hBN shown in the inset of Figure 3g after oxidation at 450 °C for 5 h. In contrast to SiO_2-supported graphene (Figure 3a,b), the phase image is homogeneous (see also phase histogram in Figure 3f), which indicates the absence of any etch pits in graphene and the significantly reduced reactivity of hBN-supported graphene.

Figure 3g shows the Raman spectra of SLG oxidized at 450 °C for 5 h at different positions between points A and B indicated in the inset. The spacing between neighboring points is 0.3 μm. Since the D band energy is dispersive with respect to the excitation energy of the laser and increases with the energy, we here used a laser wavelength of 633 nm to clearly distinguish the D peak of SLG and the peak derived from the hBN E_{2g} mode. On SiO_2 at point A we see the graphene D peak, while on hBN at point B the graphene D peak is absent and the hBN E_{2g} mode is present, suggesting the absence of defects in SLG on hBN. The region of coexistence of the D peak and the hBN E_{2g} peak in the Raman spectra is of order 1 μm wide, comparable to the laser spot size, indicating that both SiO_2-, and hBN-supported graphene are illuminated in this region. We also observe a splitting of the graphene G band into two peaks G^- (1583 cm^{-1}) and G^+ (1610 cm^{-1}) in the same intermediate region, resulting from undoped graphene on hBN and highly doped graphene on SiO_2, respectively. Splitting rather than shifting of the G peak again indicates an abrupt transition in doping from SiO_2-supported to hBN-supported graphene.

The observed reduced reactivity of SLG on hBN relative to SiO_2 can be explained by either hBN's flatness or its reduced charged inhomogeneity. To resolve this dilemma, we oxidize graphene on mica, which is atomically flat (as shown in Figure 1b) but

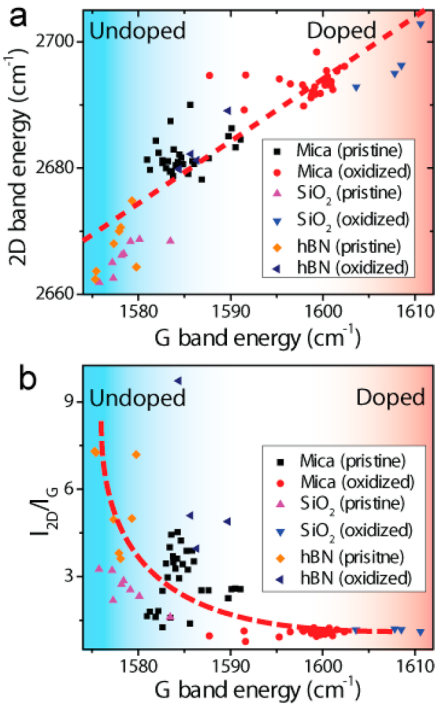

Figure 4. (a) The Raman 2D band energies of SLG on mica, hBN, and SiO_2 before and after oxidation at 500 °C as functions of the Raman G band energy. The dashed line is a linear fit with a slope of 0.98 ± 0.05. (b) The intensity ratios of the Raman 2D peak to the G peak of graphene on mica, hBN, and SiO_2 before and after oxidation at 500 °C as functions of the Raman G band energy. The dashed curved line is a guide to the eye.

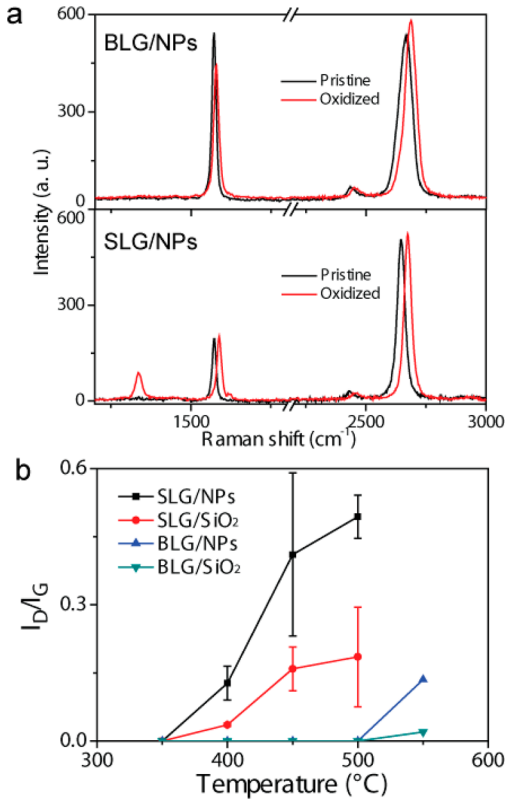

Figure 5. (a) Raman spectra of BLG (top) and SLG (bottom) on SiO_2 nanoparticles before and after oxidation at 500 °C for 2 h. (b) The intensity ratios of the Raman D peak to G peak of SLG and BLG on SiO_2 and on SiO_2 nanoparticles as functions of oxygen treatment temperature.

presumably exhibits comparable charge inhomogeneity to SiO_2-supported graphene.

As shown in Figure 2a, in contrast to hBN-supported SLG, SLG on mica is partly etched by oxidation. Thus, the flatness of graphene alone does not suppress its reactivity. We further examine the doping of graphene on mica before and after oxidation. It has been empirically demonstrated that the Raman 2D band energy increases with increasing concentration of hole carriers, showing a nearly linear relationship with the G band energy.[42] Additionally, the relative intensity of the 2D band to the G band characteristically decreases with carrier concentration.[42] Figure 4a displays the 2D band energy of SLG on SiO_2, hBN, and mica as a function of the G band energy before and after oxidation at 500 °C for 2 h. Each data point is obtained from a different graphene flake on each substrate. With oxidation, the 2D band energies of graphene on SiO_2 and on mica increase together with the G band energy. The nearly linear relationship between the 2D and G band energies, with a slope of 0.98 ± 0.05, is consistent with previous observations,[42,44] indicating hole-doping of graphene by oxidation. Graphene on hBN shows the lowest G and 2D peak positions after oxidative treatment, consistent with low reactivity. Figure 4b shows the intensity ratio of the 2D peak (I_{2D}) to the G peak (I_G) as a function of the G band energy. Each data point corresponds to a different graphene sample. The significant decrease of I_{2D}/I_G of graphene on mica and SiO_2 after oxidation also strongly supports oxidative doping of these samples. In contrast, I_{2D}/I_G for graphene on hBN shows no clear trend upon oxidation, and the higher values of I_{2D}/I_G for graphene on hBN compared to mica or SiO_2 are consistent with low oxidative reactivity.

The large reactivity of SLG on mica and its diminution with thickness as shown in Figure 2c indicates that flatness is not the reason for reduced reactivity of SLG on hBN, and we conclude that substrate charged impurities play a dominant role in controlling the reactivity of SLG on a substrate. Even though graphene is deposited onto freshly cleaved mica in a N_2 atmosphere, water layers are often trapped on mica. The water layers act to block charge transfer between charged impurities on mica and graphene.[44] The distinct morphology of mica-supported SLG after oxygen treatment in Figure 2a is presumably because the regions covering water layers on graphene are less reactive to oxygen molecules and not etched.

Finally, we probe the oxidative reactivity of graphene supported on an extremely corrugated substrate of a SiO_2 nanoparticle thin film. Figure 5a shows typical Raman spectra of SLG and BLG on SiO_2 nanoparticles

before and after oxidation at 500 °C for 2 h. After oxidation, the D peak of SLG is activated but is absent for BLG. In Figure 5b, we plot the intensity ratio of the D peak (I_D) to the G peak (I_G) of graphene on SiO_2 nanoparticles and, for comparison, on bare SiO_2 as a function of oxygen treatment temperature. On both thermally grown SiO_2 and SiO_2 nanoparticle thin films, the D peaks of SLG are activated above 400 °C. In contrast, the D peaks of BLG are not activated below 500 °C regardless of substrate. Thus, the increased reactivity of SLG relative to BLG on SiO_2 is not caused by increased corrugation on the few-nanometer length scale (see Table 1: BLG on SiO_2 nanoparticles is rougher than SLG on SiO_2 in terms of curvature and strain). We cannot completely rule out the possibility that sharp conical singularities[38] undetected by AFM are playing a role in the reactivity; however, that scenario would not explain the similar reactivity of flat graphene on mica, which should not exhibit conical singularities. The results indicate that the differences in reactivity are due to the difference in electronic structure. The increased reactivity of SLG relative to BLG is consistent with charge disorder as the cause: SLG has significantly lower density of electronic states and therefore larger fluctuations in chemical potential for a given charged impurity concentration.[20]

CONCLUSIONS

We have measured the oxidative reactivity of SLG supported on substrates with different surface roughnesses and charged impurities. SLG on flat hBN with low charged impurities shows reduced oxygen reactivity comparable to multilayer graphene, while SLG on flat mica shows reactivity similar to SLG on SiO_2, pinpointing charge disorder as the source of the increased reactivity of SLG. This is strongly supported by the observation that reactivity of graphene on SiO_2 depends on layer number (SLG *vs* BLG) but not on graphene roughness (SiO_2 nanoparticle substrates *vs* thermally grown SiO_2). Our observations may point to new strategies for using substrates to control the chemical functionalization and doping of graphene, and therefore graphene's electronic properties.[45]

METHODS

hBN flakes with a typical thickness of 9−45 nm were exfoliated onto Si substrates with an oxide layer of a thickness 300 nm from hBN powder (Momentive, PolarTherm grade PT110) using water-soluble tape (3M, water-soluble wave solder tape). Muscovite mica (Ted Pella, Inc. Highest grade V1 Mica) was cleaved immediately before depositing graphene in a glovebag filled with N_2 to minimize adsorption of water onto the mica surface. The SiO_2 nanoparticle thin films were prepared by spin-coating the nanoparticle dispersions (Nissan Chemical America Corp., SNOWTEX-O) on SiO_2 with a thickness of 300 nm. Before spin-coating, SiO_2 substrates were sufficiently wetted by isopropyl alcohol (Sigma-Aldrich, 2-propanol anhydrous 99.5%). The SiO_2 nanoparticle suspension was diluted with isopropyl alcohol to ~5 wt %. The spin-coating was performed at 4000 rpm for 30 s. Graphene was mechanically exfoliated from Kish graphite using water-soluble tape. The samples were then annealed in an Ar/O_2 mixture at temperatures ranging from 350 to 600 °C for 2−5 h in a quartz furnace. The flow rates of Ar and O_2 were 1.0 L/min and 0.7 L/min, respectively. Raman spectroscopy was carried out with a wavelength of excitation laser 532 and 633 nm. The laser spot size was ~1 μm. AFM measurements were performed in tapping mode in ambient using silicon cantilevers with a nominal tip radius of <10 nm (Nanoworld, NCH-20).

Conflict of Interest: The authors declare no competing financial interest.

Acknowledgment. This work was supported by the University of Maryland NSF-MRSEC under Grant No. DMR 05-20471, NSF under Grant No. DMR 08-04976, and the U.S. ONR MURI. Additional infrastructure support provided by the UMD NanoCenter and CNAM. We thank Momentive Performance Materials, Inc. for providing samples of boron nitride powder, and Nissan Chemical America Corporation for providing silica nanoparticles dispersions.

Supporting Information Available: Height profile analysis of AFM images, definitions of the rms roughness and the characteristic length of graphene surfaces, the dispersive behavior of the Raman D mode of graphene and the nondispersive behavior of E_{2g} Raman mode of hBN, and AFM height, and phase images of pristine graphene on SiO_2. This material is available free of charge *via* the Internet at http://pubs.acs.org.

REFERENCES AND NOTES

1. Boukhvalov, D. W.; Katsnelson, M. I. Chemical Functionalization of Graphene. *J. Phys.; Condens. Matter.* **2009**, *21*, 344205.
2. Loh, K. P.; Bao, Q.; Ang, P. K.; Yang, J. The Chemistry of Graphene. *J. Mater. Chem.* **2010**, *20*, 2277–2289.
3. Liu, H.; Liu, Y.; Zhu, D. Chemical Doping of Graphene. *J. Mater. Chem.* **2011**, *21*, 3335–3345.
4. Ryu, S.; Han, M. Y.; Maultzsch, J.; Heintz, T. F.; Kim, P.; Steigerwald, M. L.; Brus, L. E. Reversible Basal Plane Hydrogenation of Graphene. *Nano Lett.* **2008**, *8*, 4597–4602.
5. Elias, D. C.; Nair, R. R.; Mohiuddin, T. M. G.; Morozov, S. V.; Blake, P.; Halsall, M. P.; Ferrari, A. C.; Boukhvalov, D. W.; Katsnelson, M. I.; Geim, A. K.; *et al.* Control of Graphene's Properties by Reversible Hydrogenation: Evidence for Graphane. *Science* **2009**, *323*, 610–613.
6. Robinson, J. T.; Burgess, J. S.; Junkermeier, C. E.; Badescu, S. C.; Reinecke, T. L.; Perkins, F. K.; Zalalutdniov, M. K.; Baldwin, J. W.; Culbertson, J. C.; Sheehan, P. E.; *et al.* Properties of Fluorinated Graphene Films. *Nano Lett.* **2010**, *10*, 3001–3005.
7. Nair, R. R.; Ren, W.; Jalil, R.; Riaz, I.; Kravets, V. G.; Britnell, L.; Blake, P.; Schedin, F.; Mayorov, A. S.; Yuan, S.; *et al.* Fluorographene: A Two-Dimensional Counterpart of Teflon. *Small* **2010**, *6*, 2877–2884.
8. Nair, R. R.; Sepioni, M.; Tsai, I.-L.; Lehtinen, O.; Keinonen, J.; Krasheninnikov, A. V.; Thomson, T.; Geim, A. K.; Grigorieva, I. V. Spin-Half Paramagnetism in Graphene Induced by Point Defects. *Nat. Phys.* **2012**, *8*, 199–202.
9. Jung, N.; Kim, N.; Jockusch, S.; Turro, N. J.; Kim, P.; Brus, L. Charge Transfer Chemical Doping of Few Layer Graphenes: Charge Distribution and Band Gap Formation. *Nano Lett.* **2009**, *9*, 4133–4137.
10. Wang, X.; Li, X.; Zhang, L.; Yoon, Y.; Weber, P. K.; Wang, H.; Guo, J.; Dai, H. N-Doping of Graphene Through Electrothermal Reactions with Ammonia. *Science* **2009**, *324*, 768–771.

11. Boukhvalov, D. W.; Katsnelson, M. I. Chemical Functionalization of Graphene with Defects. *Nano Lett.* **2008**, *8*, 4373–4379.
12. Liu, L.; Ryu, S.; Tomasik, M. R.; Stolyarova, E.; Jung, N.; Hybertsen, M. S.; Steigerwald, M. L.; Brus, L. E.; Flynn, G. W. Graphene Oxidation: Thickness-Dependent Etching and Strong Chemical Doping. *Nano lett.* **2008**, *8*, 1965–1970.
13. Sharma, R.; Baik, J. H.; Perera, C. J.; Strano, M. S. Anomalously Large Reactivity of Single Graphene Layers and Edges toward Electron Transfer Chemistries. *Nano Lett.* **2010**, *10*, 398–405.
14. Koehler, F. M.; Jacobsen, A.; Ensslin, K.; Stampfer, C.; Stark, W. J. Selective Chemical Modification of Graphene Surfaces: Distinction between Single- and Bilayer Graphene. *Small* **2010**, *6*, 1125–1130.
15. Martin, J.; Akerman, N.; Ulbricht, G.; Lohmann, T.; Smet, J. H.; von Klitzing, K.; Yacoby, A. Observation of Electron-Hole Puddles in Graphene Using a Scanning Single-Electron Transistor. *Nat. Phys.* **2008**, *4*, 144–148.
16. Zhang, Y.; Brar, V. W.; Girit, C.; Zettl, A.; Crommie, M. F. Origin of Spatial Charge Inhomogeneity in Graphene. *Nat. Phys.* **2009**, *5*, 722–726.
17. Tan, Y.-W.; Zhang, Y.; Bolotin, K.; Zhao, Y.; Adam, S.; Hwang, E. H.; Das Sarma, S.; Stormer, H. L.; Kim, P. Measurement of Scattering Rate and Minimum Conductivity in Graphene. *Phys. Rev. Lett.* **2007**, *99*, 246803.
18. Chen, J.-H.; Jang, C.; Adam, S.; Fuhrer, M. S.; Williams, E. D.; Ishigami, M. Charged-Impurity Scattering in Graphene. *Nat. Phys.* **2008**, *4*, 377–381.
19. Jang, C.; Adam, S.; Chen, J.-H.; Williams, E. D.; Das Sarma, S.; Fuhrer, M. S. Tuning the Effective Fine Structure Constant in Graphene: Opposing Effects of Dielectric Screening on Short- and Long-Range Potential Scattering. *Phys. Rev. Lett.* **2008**, *101*, 146805.
20. Adam, S.; Das Sarma, S. Boltzmann Transport and Residual Conductivity in Bilayer Graphene. *Phys. Rev. B* **2008**, *77*, 115436.
21. Pietronero, L.; Strässler, S.; Zeller, H. R.; Rice, M. J. Charge Distribution in *c* Direction in Lamellar Graphite Acceptor Intercalation Compounds. *Phys. Rev. Lett.* **1978**, *41*, 763–767.
22. Datta, S. S.; Strachan, D. R.; Mele, E. J.; Johnson, A. T. C. Surface Potentials and Layer Charge Distributions in Few-Layer Graphene Films. *Nano Lett.* **2009**, *9*, 7–11.
23. Boukhvalov, D. W.; Katsnelson, M. I. Enhancement of Chemical Activity in Corrugated Graphene. *J. Phys. Chem. C.* **2009**, *113*, 14176–14178.
24. Ishigami, M.; Chen, J. H.; Cullen, W. G.; Fuhrer, M. S.; Williams, E. D. Atomic Structure of Graphene on SiO_2. *Nano Lett.* **2007**, *7*, 1643–1648.
25. Cullen, W. G.; Yamamoto, M.; Burson, K. M.; Chen, J. H.; Jang, C.; Li, L.; Fuhrer, M. S.; Williams, E. D. High-Fidelity Conformation of Graphene to SiO_2 Topographic Features. *Phys. Rev. Lett.* **2010**, *105*, 215504.
26. Kim, E.-A.; Castro Neto, A. H. Graphene as an Electronic Membrane. *Europhys. Lett.* **2008**, *84*, 57007.
27. Locatelli, A.; Knox, K. R.; Cvetko, D.; Menteş, T. O.; Niño, M. A.; Wang, S.; Yilmaz, M. B.; Kim, P.; Osgood, R. M., Jr.; Morgante, A. Corrugation in Exfoliated Graphene: An Electron Microscopy and Diffraction Study. *ACS Nano* **2010**, *4*, 4879–4889.
28. Yamamoto, M.; Pierre-Louis, O.; Huang, J.; Fuhrer, M. S.; Einstein, T. L.; Cullen, W. G. Princess and the Pea at the Nanoscale: Wrinkling and Unbinding of Graphene on Nanoparticles. *Condens Matter*, arXiv:1201.5667 .
29. Fan, X.; Nouchi, R.; Tanigaki, K. Effect of Charge Puddles and Ripples on the Chemical Reactivity of Single Layer Graphene Supported by SiO_2/Si Substrate. *J. Phys. Chem. C.* **2011**, *115*, 12960–12964.
30. Xue, J.; Sanchez-Yamagishi, J.; Bulmash, D.; Jacquod, P.; Deshpande, A.; Watanabe, K.; Taniguchi, T.; Jarillo-Herrero, P.; LeRoy, B. J. Scanning Tunneling Microscopy and Spectroscopy of Ultra-flat Graphene on Hexagonal Boron Nitride. *Nat. Mater.* **2011**, *10*, 282–285.
31. Decker, R.; Wang, Y.; Brar, V. W.; Regan, W.; Tsai, H.-Z.; Wu, Q.; Gannett, W.; Zettl, A.; Crommie, M. F. Local Electronic Properties of Graphene on a BN Substrate *via* Scanning Tunneling Microscopy. *Nano Lett.* **2011**, *11*, 2291–2295.
32. Dean, C. R.; Young, A. F.; Meric, I.; Lee, C.; Wang, L.; Sorgenfrei, S.; Watanabe, K.; Taniguchi, T.; Kim, P.; Shepard, K. L.; *et al*. Boron Nitride Substrates for High-Quality Graphene Electronics. *Nat. Nanotechnol.* **2010**, *5*, 722–726.
33. Rudenko, A. N.; Keil, F. J.; Katsnelson, M. I.; Lichtenstein, A. I. Graphene Adhesion on Mica: Role of Surface Morphology. *Phys. Rev. B* **2011**, *83*, 045409.
34. Ponomarenko, L. A.; Yang, R.; Mohiuddin, T. M.; Katsnelson, M. I.; Novoselov, K. S.; Morozov, S. V.; Zhukov, A. A.; Schedin, F.; Hill, E. W.; Geim, A. K. Effect of a High-κ Environment on Charge Carrier Mobility in Graphene. *Phys. Rev. Lett.* **2009**, *102*, 206603.
35. Lui, C. H.; Liu, L.; Mak, K. F.; Flynn, G. W.; Heinz, T. F. Ultraflat Graphene. *Nature* **2009**, *462*, 339–341.
36. Zomer, P. J.; Dash, S. P.; Tombros, N.; van Wees, B. J. A Transfer Technique for High Mobility Graphene Devices on Commercially Available Hexagonal Boron Nitride. *Appl. Phys. Lett.* **2011**, *99*, 232104.
37. Xu, K.; Cao, P.; Heath, J. R. Graphene Visualizes the First Water Adlayers on Mica at Ambient Conditions. *Science* **2010**, *329*, 1188–1191.
38. Pereira, V. M.; Castro Neto, A. H.; Liang, H. Y.; Mahadevan, L. Geometry, Mechanics, and Electronics of Singular Structures and Wrinkles in Graphene. *Phys. Rev. Lett.* **2010**, *105*, 156603.
39. Ryu, S.; Liu, L; Berciaud, S.; Yu, Y.-J.; Liu, H.; Kim, P.; Flynn, G. W.; Brus, L. E. Atmospheric Oxygen Binding and Hole Doping in Deformed Graphene on a SiO_2 Substrate. *Nano Lett.* **2010**, *10*, 4944–4951.
40. Hossain, M. Z.; Johns, J. E.; Bevan, K. H.; Karmel, H. J.; Liang, Y. T.; Yoshimoto, S.; Mukai, K.; Koitaya, T.; Yoshinobu, J.; Kawai, M.; *et al*. Chemically Homogeneous and Thermally Reversible Oxidation of Epitaxial Graphene. *Nat. Chem.* **2012**, *4*, 305–309.
41. Yan, J.; Zhang, Y.; Kim, P.; Pinczuk, A. Electric Field Effect Tuning of Electron-Phonon Coupling in Graphene. *Phys. Rev. Lett.* **2007**, *98*, 166802.
42. Das, A.; Pisana, S.; Chakraborty, B.; Piscanec, S.; Saha, S. K.; Waghmare, U. V.; Novoselov, K. S.; Krishnamurthy, H. R.; Geim, A. K.; Ferrari, A. C.; *et al*. Monitoring Dopants by Raman Scattering in an Electrochemically Top-Gated Graphene Transistor. *Nat. Nanotechnol.* **2008**, *3*, 210–215.
43. Geick, R.; Perry, C. H.; Rupprecht, G. Normal Modes in Hexagonal Boron Nitride. *Phys. Rev.* **1966**, *146*, 543–547.
44. Shim, J.; Lui, C. H.; Ko, T. Y.; Yu, Y.-J.; Kim, P.; Heinz, T. F.; Ryu, S. Water-Gated Charge Doping of Graphene Induced by Mica Substrates. *Nano Lett.* **2012**, *12*, 648–654.
45. Note added. After submission of this manuscript, we became aware of similar work by other groups.[46,47]
46. Garcia, A. G. F.; Neumann, M.; Amet, F.; Williams, J. R.; Watanabe, K.; Taniguchi, T.; Goldhaber-Gordon, D. Effective Cleaning of Hexagonal Boron Nitride for Graphene Devices. *Nano Lett.* Published online August 6, 2012, doi: 10.1021/nl3011726.
47. Wang, Q. H.; Jin, Z.; Kim, K. K.; Hilmer, A. J.; Paulus, G. L. C.; Shih, C.-J.; Ham, M.-H.; Sanchez-Yamagishi, J. D.; Watanabe, K.; Taniguchi, T. *et al*. Understanding and Controlling the Substrate Effect on Graphene Electron-Transfer Chemistry *via* Reactivity Imprint Lithography. *Nat. Chem.* Published online August 12, 2012, doi: 10.1038/nchem.1421.